SUPERCONDUCTIVITY

Time-reversal symmetry-breaking superconductivity in epitaxial bismuth/nickel bilayers

Xinxin Gong,[1,2] Mehdi Kargarian,[3] Alex Stern,[1] Di Yue,[2] Hexin Zhou,[2] Xiaofeng Jin,[2] Victor M. Galitski,[3] Victor M. Yakovenko,[3] Jing Xia[1]*

Superconductivity that spontaneously breaks time-reversal symmetry (TRS) has been found, so far, only in a handful of three-dimensional (3D) crystals with bulk inversion symmetry. We report an observation of spontaneous TRS breaking in a 2D superconducting system without inversion symmetry: the epitaxial bilayer films of bismuth and nickel. The evidence comes from the onset of the polar Kerr effect at the superconducting transition in the absence of an external magnetic field, detected by the ultrasensitive loop-less fiber-optic Sagnac interferometer. Because of strong spin-orbit interaction and lack of inversion symmetry in a Bi/Ni bilayer, superconducting pairing cannot be classified as singlet or triplet. We propose a theoretical model where magnetic fluctuations in Ni induce the superconducting pairing of the $d_{xy} \pm id_{x^2-y^2}$ orbital symmetry between the electrons in Bi. In this model, the order parameter spontaneously breaks the TRS and has a nonzero phase winding number around the Fermi surface, thus making it a rare example of a 2D topological superconductor.

INTRODUCTION

Unconventional superconductors, characterized by spontaneous breaking of additional symmetries other than U(1) gauge symmetry, often have novel properties and reveal new physics. Spontaneous time-reversal symmetry breaking (TRSB) in a superconducting state is one of the most fascinating phenomena. Such superconductors may host unusual particles called Majorana fermions (*1*), much discussed for topological quantum computing (*2*). However, up to now, spontaneous TRSB has been observed only in a few three-dimensional (3D) superconductors with bulk inversion symmetry, such as Sr_2RuO_4, UPt_3, and URu_2Si_2 (*3*–*5*). The possibility of spontaneous TRSB has not been investigated experimentally, so far, for a 2D surface superconductivity at interfaces between nonsuperconducting materials (*6*), which are currently attracting a lot of interest for possible device applications. These 2D superconducting systems typically lack inversion symmetry because of the difference between the top and bottom surroundings of the layer. Because of the spin-orbit interaction, the spin degeneracy of the electronic states is lifted in these noncentrosymmetric materials, thus making the usual singlet-triplet classification of superconducting pairing inapplicable (*7*). Recent progress in the fabrication of high-quality heterostructures enables artificial realization of these exotic superconducting states. Here, we report an observation of spontaneous TRSB in the superconducting state of a 2D epitaxially grown bilayer made from the nonsuperconducting elements Bi and Ni.

The bulk rhombohedral crystalline Bi, which is the heaviest nonradioactive element in the periodic table and a semimetal with an extremely long mean free path, is not superconducting at temperatures down to 50 mK (*8*). Thus, it was a complete surprise when tunneling experiments (*9*, *10*) identified a superconducting transition at $T_c = 3.6$ K in Bi thin films evaporated on a thin seed layer of ferromagnetic Ni. It is unknown what the symmetry of this superconducting pairing is and, in particular, whether it breaks the time-reversal symmetry (TRS). Because of the recent progress in epitaxial film technology, it became possible to fabricate high-quality superconducting Bi/Ni films (*11*) suitable for optical measurements of the polar Kerr effect (PKE). The PKE can be used for experimental detection of spontaneous TRSB at a superconducting transition, as it has been demonstrated for Sr_2RuO_4, UPt_3, and URu_2Si_2 (*3*–*5*). The PKE measures the optical phase difference between two opposite circular polarizations of light reflected on a sample surface, thus giving information about the TRS of the system. For optical frequencies ω, which are much higher than the superconducting gap Δ, the Kerr signal θ_K is expected (*12*) to be proportional to $(\Delta/\omega)^2$ and is generally less than 1 μrad (10^{-9} rad) (*3*, *4*). To measure such a small θ_K, we used a custom-made ultrasensitive loop-less fiber-optic Sagnac interferometer (see fig. S1) (*12*, *13*). The geometry and design of the Sagnac interferometer (*12*) guarantee that all the time reversal–invariant effects (such as optical birefringence, temperature fluctuations, and mechanical vibrations) cancel out, and a nonzero signal θ_K appears only if the measured sample breaks the TRS. This method (*14*, *15*) probes the sample at an optical penetration depth of a few tens of nanometer and is ideally suited for studying thin films.

RESULTS AND DISCUSSION

The Bi(110)/Ni(001) samples were fabricated using molecular beam epitaxy on MgO(001) substrate (see fig. S2) and then mounted in an optical cryostat, with the optical probe beam incident normally on the sample surface for the PKE measurements, as shown in Fig. 1A. Four gold wires were attached to the sample surface with silver epoxy for transport measurements. A study of thickness dependence (see fig. S4) shows that an increase in the thickness of the face-centered cubic (fcc) Ni layer suppresses T_c, whereas an increase in Bi thickness restores T_c back to 4.1 K. These observations (*11*) suggest that although the presence of Ni is necessary for providing the pairing interaction in Bi, superconductivity does not develop at the direct Bi/Ni interface because of the strong ferromagnetism of Ni but, instead, develops at the opposite surface of Bi facing the vacuum. A further increase of Bi thickness starts to suppress T_c (*11*), as expected for going toward the limit of bulk Bi. Also, there is an optimal Bi layer thickness for maximal T_c. In this experiment, we choose a Bi thickness of about 20 nm to minimize the Kerr signal from the underlying Ni layer while maintaining the optimal $T_c = 4.1$ K.

Our experimental setup allows us to perform optical measurements on both the Bi and Ni sides of the bilayer, as shown in Fig. 1 (B and C).

[1]Department of Physics and Astronomy, University of California, Irvine, Irvine, CA 92697, USA. [2]Department of Physics, Fudan University, Shanghai 200433, China. [3]Department of Physics, Condensed Matter Theory Center and Joint Quantum Institute, University of Maryland, College Park, MD 20742, USA.
*Corresponding author. Email: xia.jing@uci.edu

The main results of the paper are the measurements on the Bi side shown in Fig. 1B. The Bi (25 nm)/Ni (2 nm) sample was cooled at zero magnetic field (<0.1 Oe) to the base temperature of the cryostat and then measured upon warming in zero field (ZF). The onset of the ZF Kerr signal is observed at 4.1 K, which coincides with the superconducting transition, as signaled by the initial drop of resistance, thus demonstrating that spontaneous TRSB is due to superconductivity. The Kerr signal θ_K becomes larger at lower temperatures, reaching 120 nrad at $T = 3$ K. The dashed line is a guide to the eye of the form of $1 - (T/T_c)^2$ (*16*). Each Kerr angle θ_K data point represents an average of 1000 s, with the error bar denoting the statistical uncertainty of less than 10 nrad. The systematic source of error/uncertainty is mainly the long-term drift of the interferometer, which is estimated to be 5 nrad. The Sagnac interferometer operates at an optical power of 2 μW to prevent any optical heating (*3*, *4*) of the sample.

One may ask whether the observed onset of the Kerr signal at 4.1 K on the Bi side of the sample could somehow originate from the ferromagnetic Ni on the other side. We believe this is not the case because of the following reasons. First, the 400-K ferromagnetic Curie temperature of Ni is two orders of magnitude greater than the 4.1-K onset temperature of PKE on the Bi side; thus, it is unlikely that the two effects are related. Second, the magnetic moment of Ni is almost parallel to the interface surface, whereas the PKE is sensitive only to the perpendicular component. Third, the opacity and thickness of the Bi layer greatly suppress an optical pickup of a signal originating from the Ni side. Nevertheless, to rule out the possibility that a yet-unknown magnetic transition in the underlying Ni layer at 4.1 K generates the Kerr signal on the Bi side, we have directly measured the PKE on the Ni side by flipping the sample, as shown in Fig. 1C. Thin Ni films are known to have an almost in-plane magnetic anisotropy; hence, the magnetic moment of Ni is almost in the plane, resulting in near-zero polar Kerr signal. This is shown by the blue curve in Fig. 1C, where a temperature-independent θ_K of 0.75 μrad is observed without any sign of transition at 4.1 K. When a strong magnetic field of 1600 Oe is applied perpendicularly to the interface, the majority of the magnetic moment of Ni is out of the plane. In addition, the corresponding perpendicular component produces a Kerr signal of 130 μrad, as shown by the red curve in Fig. 1C. These indicate a magnetic anisotropy angle of less than 0.33° from the in-plane direction, which is common for thin Ni films (*10*). During the Kerr measurement on the Bi side, because only a tiny fraction of the light could penetrate into the underlying Ni layer, the Kerr signal is less than 5 μrad, or 4% of the Kerr signal from the Ni side. Therefore, if the 120-nrad Kerr signal in Fig. 1B was due to an unknown magnetic transition in Ni at 4.1 K, it would necessarily require an increase of the Kerr signal on the Ni side by 3 μrad at a temperature below 4.1 K, which is nonexistent in the blue curve in Fig. 1C up to a precision of 0.1 μrad.

Because of spontaneous symmetry breaking, the sign of the Kerr signal observed below T_c may be positive or negative, but it can be controlled by applying a small external "training" magnetic field when cooling through the superconducting transition. Such a training effect has been observed in other TRSB superconductors (*3*–*5*), and we also find it in Bi/Ni. As shown in Fig. 2 (A and B), a Bi (20 nm)/Ni (2 nm) sample was cooled down to the lowest temperature in a magnetic field of +190 or −70 Oe perpendicular to the film, and then the Kerr signal was measured on warm-up in zero magnetic field. We observed that the sign of the Kerr signal on warm-up corresponds to the sign of the training field applied during cooldown, thus indicating that the TRSB

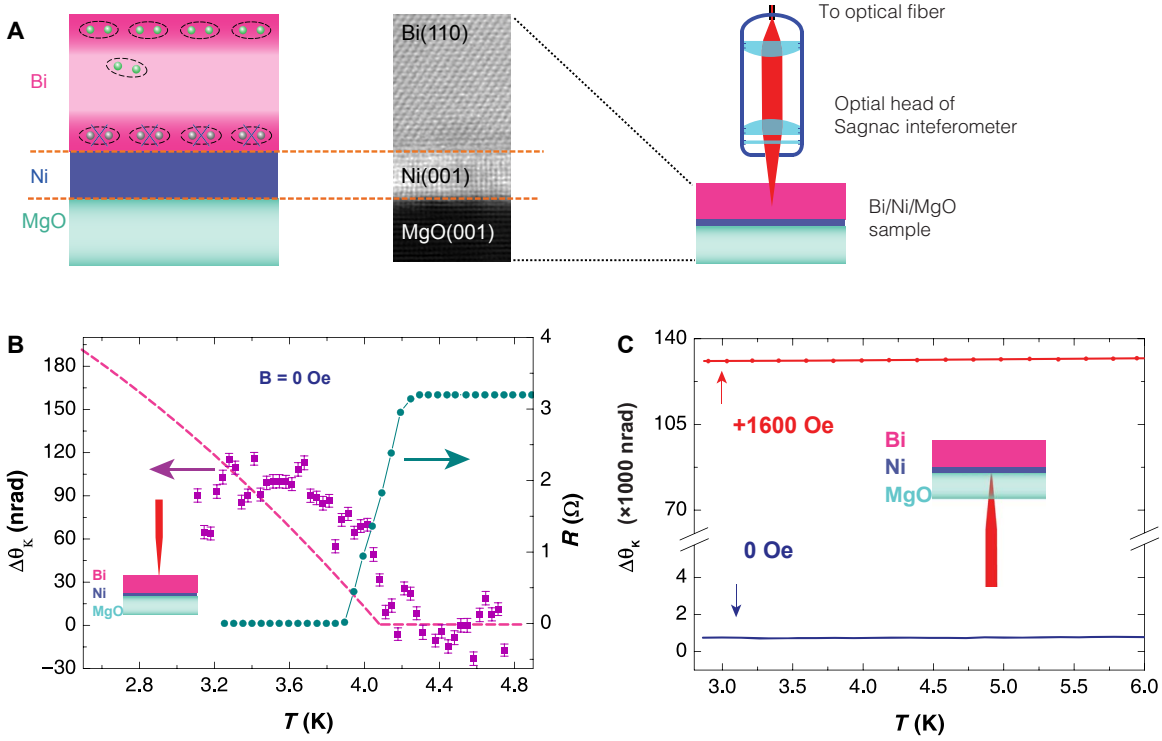

Fig. 1. Structure and Kerr signal of a Bi (25 nm)/Ni (2 nm) sample. (**A**) Left: Side view of the sample structure with a transmission electron microscopy image. Right: Schematic diagram of Kerr rotation measurement. (**B**) Kerr angle (purple) and resistance (green) measured on the Bi side for ZF cooldown, showing the onset of θ_K at $T_c = 4.1$ K. The pink dashed line is a guide to the eye with the form of $1 - (T/T_c)^2$. (**C**) Kerr signal measured on the Ni side at 1600-Oe applied perpendicular magnetic field (red) or at ZF (blue). In either case, no change of the Kerr signal was observed across $T_c = 4.1$ K.

order parameter couples to the external magnetic field. We have repeated these measurements with training fields up to 230 Oe and found the absolute values of θ_K at 2.8 K to be identical within the 20-nrad measurement uncertainty. The fact that $|\theta_K|$ is independent of the cooling field magnitude implies that the trapped superconducting flux is not responsible for the observed θ_K, because the number of trapped vortices would scale with the cooling field. The applied training magnetic fields are also too small to alter the small out-of-plane component of an Ni magnetic moment.

For a cooldown in zero magnetic field, we expect that chiral domains with positive (+) and negative (−) signs of the Kerr signal should coexist in the sample. If the optical spot is positioned within a single chiral domain, the full Kerr signal would be observed, which we believe is the case for the measurement performed without a training field (Fig. 1B). However, more often, the measured θ_K is an average of chiral domains under the focused optical spot of the diameter $w \approx 2$ μm, with a value between $+\theta_0$ and $-\theta_0$, where $\theta_0 = 60$ nrad is the value for a single domain (that is, after being trained). This is observed in 11 measurements of the Bi (20 nm)/Ni (2 nm) sample (Fig. 2C). The standard deviation $\sigma(\theta_K)$ between these measurements has two contributions: σ_0 due to random chiral domains and σ_{app} from the apparatus uncertainty. Above T_c, there is no TRSB, and $\sigma(\theta_K)$ remains constant at $\sigma_{app} = 18$ nrad. Below T_c, the TRSB occurs, and $\sigma(\theta_K)$ increases toward $\sigma_{3K} = 30$ nrad at $T = 3$ K (Fig. 2D). Therefore, σ_0 can be estimated to be 24 nrad at $T = 3$ K. By assuming 2D domains with the average size d, we estimate that $d \approx w \times \sigma_0/\theta_0 \approx 0.8$ μm.

To explain the experimental results, we propose a minimal model involving electronic surface states of Bi that interact with fluctuating magnetic moments of Ni (technical details are given in the Supplementary Materials). There are indications (*17*) that electronic states in the interior of a Bi film are gapped, and the only metallic states are the surface states. Thus, we only consider the Bi surface exposed to vacuum, because the surface exposed to Ni does not contribute to superconductivity, according to Gong *et al.* (*11*). The (110) surface of Bi may contain multiple Fermi pockets (*18*–*22*); however, we only consider the largest pocket enclosing the surface Brillouin zone center $\bar{\Gamma}$. Because of the strong Rashba-type spin-orbit coupling, the electron spin and momentum are locked on this pocket, as shown in Fig. 3A. To simplify the presentation, we assume rotational symmetry in the (x, y) plane of the surface (anisotropy is discussed at the end) and use the standard Rashba Hamiltonian $v_F(\mathbf{k} \times \boldsymbol{\sigma}) \cdot \hat{\mathbf{z}}$, where $\mathbf{k}$ and $\boldsymbol{\sigma}$ are the momentum and spin operators for 2D electrons, respectively. The Zeeman term $-\mathbf{M} \cdot \boldsymbol{\sigma}$ due to the in-plane magnetization $\mathbf{M}$ of the Ni can be eliminated by the gauge transformation $\Psi = e^{-i\mathbf{w}\cdot\mathbf{r}}\Psi'$ of the electron fields, which is equivalent to a redefinition of the electron momentum $\mathbf{p} = \mathbf{k} - \mathbf{w}$ and

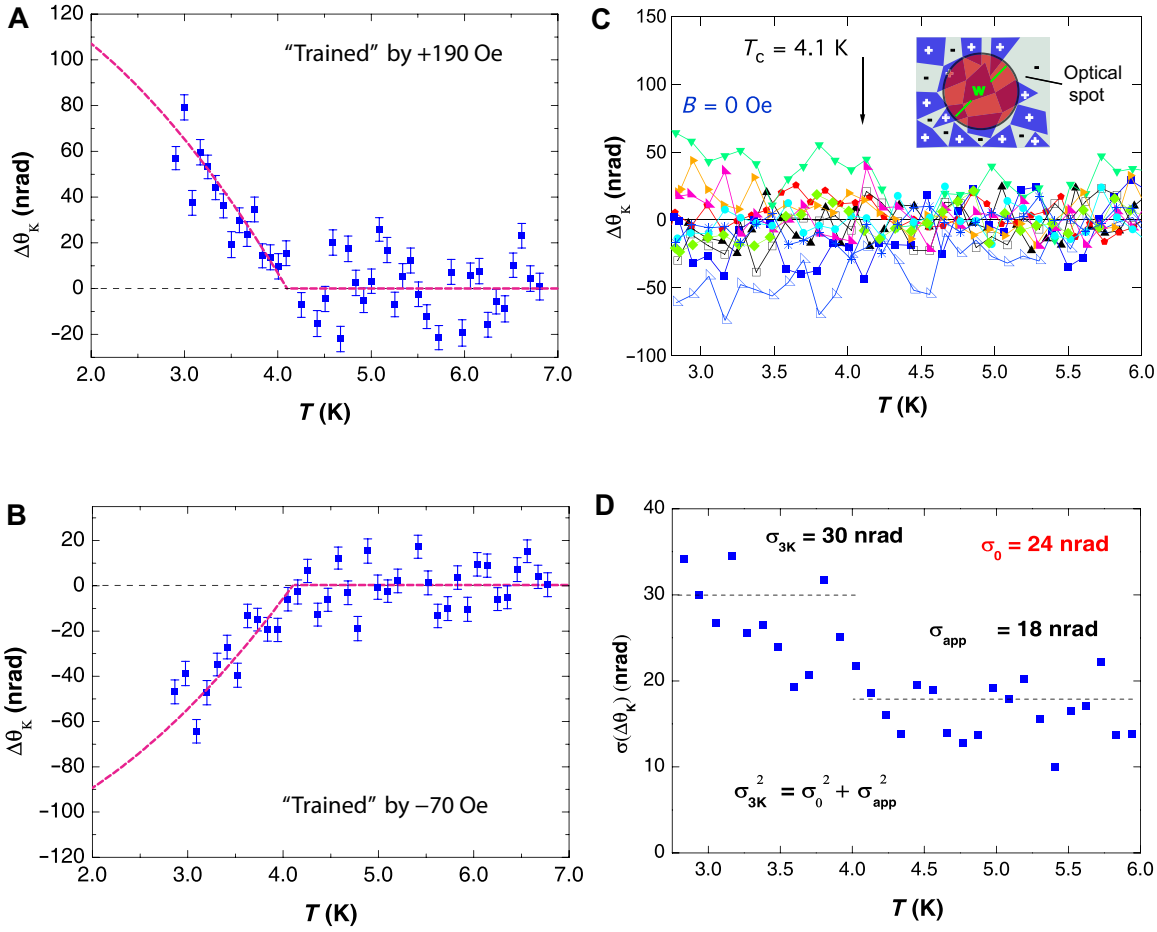

Fig. 2. Chirality training and domain size estimation of a Bi (20 nm)/Ni (2 nm) sample. (**A**) ZF warm-up data after cooling down in +190-Oe magnetic field. (**B**) ZF warm-up data after cooling in −70-Oe magnetic field. Pink dashed lines in (A) and (B) are guides to the eye with the form of $1 - (T/T_c)^2$. (**C**) Kerr effect θ_K measured during ZF warm-up, after cooling down in ZF. Inset: Random (2D) chiral domains under the optical spot. (**D**) SD $\sigma(\theta_K)$ between experiments that contain two random contributions: σ_0 due to chiral domains and σ_{app} from the apparatus.

a shift of the Fermi surface center from $\bar{\Gamma}$ to $\bar{\Gamma}'$ by the vector $\mathbf{w} = (\mathbf{M} \times \hat{\mathbf{z}})/\upsilon_F$, as shown in Fig. 3A. Then, we consider the superconducting pairing of the electrons with the opposite momenta $\mathbf{p}$ and $-\mathbf{p}$ relative to $\bar{\Gamma}'$ (Fig. 3B), which corresponds to a pairing with the total momentum $2\mathbf{w}$ relative to $\bar{\Gamma}$.

Because of the strong spin-orbit interaction and the lack of inversion symmetry (signified by the $\hat{\mathbf{z}}$ direction perpendicular to the surface), the electron states are nondegenerate for each momentum $\mathbf{p}$. Symmetry classification of 2D superconducting pairing in this case (*23*) differs substantially from the conventional, spin-degenerate case. In particular, classification into singlet and triplet pairing is not appropriate (*24*). With the spin quantization axis taken along the $\hat{\mathbf{z}}$ direction, the electron state of the momentum $\mathbf{p}$ is the spinor $|\mathbf{p}\rangle = (1, ie^{i\phi_\mathbf{p}})/\sqrt{2}$, where $\phi_\mathbf{p}$ is the azimuthal angle of the vector $\mathbf{p}$ in Fig. 3A. The time-reversed state $|\tilde{\mathbf{p}}\rangle = \Theta|\mathbf{p}\rangle$ produced by the time-reversal operator $\Theta = i\sigma^y\mathcal{K}$, where $\mathcal{K}$ is the complex conjugation and $i\sigma^y$ is the spinor metric tensor, has the momentum $-\mathbf{p}$; thus, $|\tilde{\mathbf{p}}\rangle = \eta_\mathbf{p}|-\mathbf{p}\rangle$, where $\eta_\mathbf{p} = -ie^{-i\phi_\mathbf{p}}$ is a phase factor. Because $\Theta^2 = -1$ for spin 1/2, the phase factor has the property $\eta_\mathbf{p} = -\eta_{-\mathbf{p}}$ (which can also be checked using $\phi_{-\mathbf{p}} = \phi_\mathbf{p} + \pi$) and cannot be eliminated by any gauge transformation. The corresponding second-quantized operators also involve this phase factor: $\tilde{\psi}_\mathbf{p} = \Theta\psi_\mathbf{p}\Theta^{-1} = \eta^*_\mathbf{p}\psi_{-\mathbf{p}}$. Following the study by Samokhin (*23*), the superconducting condensate $f(\mathbf{p}) = \langle\psi_\mathbf{p}\tilde{\psi}_\mathbf{p}\rangle$ is introduced for the fermion fields that are time-reversal partners of each other. An important observation is that $f(\mathbf{p})$ is an even function of $\mathbf{p}$: $f(\mathbf{p}) = \eta^*_\mathbf{p}\langle\psi_\mathbf{p}\psi_{-\mathbf{p}}\rangle = -\eta^*_\mathbf{p}\langle\psi_{-\mathbf{p}}\psi_\mathbf{p}\rangle = -\eta^*_\mathbf{p}\eta_{-\mathbf{p}}\langle\psi_{-\mathbf{p}}\tilde{\psi}_{-\mathbf{p}}\rangle = \langle\psi_{-\mathbf{p}}\tilde{\psi}_{-\mathbf{p}}\rangle = f(-\mathbf{p})$, where fermion anticommutation was used. Thus, only even values of m are permitted in the expansion $f(\mathbf{p}) = \Sigma_m f_m e^{im\phi_\mathbf{p}}$ over circular harmonics for a rotationally invariant system (because $\phi_{-\mathbf{p}} = \phi_\mathbf{p} + \pi$). The simplest case $m = 0$, studied by Gor'kov and Rashba (*24*), represents a pairing that is rotationally and time reversal–invariant. The $p_x \pm ip_y$ pairing with the odd $m = \pm 1$, often discussed for Sr_2RuO_4, is forbidden in the nondegenerate case.

To explain spontaneous TRSB in Bi/Ni bilayers, we propose that the superconducting pairing in this system takes place with $m = \pm 2$, where the sign is either selected spontaneously or controlled by a small training magnetic field, as shown in Fig. 3B. The pairing states with $m = \pm 2$, which can be also labeled as $d_{xy} \pm id_{x^2-y^2}$, are the time-reversal partners of each other. As shown in the study by Samokhin (*23*), these states have two chiral Majorana edge modes propagating around the sample edge, either clockwise or counterclockwise. In the conventional spinor basis, the superconducting condensate $F_{\alpha\beta}(\mathbf{p}) = \langle\Psi_{\mathbf{p}\alpha}\Psi_{-\mathbf{p}\beta}\rangle$ is a 2×2 matrix labeled by spin indices $\alpha, \beta = \uparrow, \downarrow$. Although the spin S_z and orbital angular momentum L_z have different values for different components of this matrix, representing a mix of singlet and triplet pairing, the total angular momentum has the same value $J_z = S_z + L_z = m = \pm 2$ for all matrix components. Similar conclusions were obtained by Vafek and Wang (*25*) using renormalization group for repulsive interaction between electrons. In a less-convenient representation used in the studies by Farrell and Pereg-Barnea (*26*) and Sergienko and Curnoe (*27*), the pairing function $\langle\psi_\mathbf{p}\psi_{-\mathbf{p}}\rangle = \eta_\mathbf{p} f(\mathbf{p})$ has the winding number $m - 1$, with the values 1 and −3 (corresponding to p- and f-wave pairing) for the time-reversed pairings with the total angular momentum $J_z = m = \pm 2$.

It was shown in the study by Scheurer (*28*) that phonons cannot possibly produce the TRSB superconductivity. Thus, we propose that the superconducting pairing of the surface electron states in the Bi layer is mediated by magnetic fluctuations in the Ni layer. This scenario is supported by the observation (*11*) that superconductivity exists only for very thin Ni layers and is suppressed with the increase of Ni thickness, which would reduce magnetic fluctuations. We particularly focus on the out-of-plane fluctuations of the Ni magnetic moments [the effect of in-plane fluctuations is discussed in the study by Kargarian *et al.* (*29*)]. The effective interaction in the Cooper channel between electrons with the momenta $\mathbf{p}$ and $\mathbf{p}'$ is given by the properly symmetrized product of the magnon propagator $D(\mathbf{p} - \mathbf{p}')$ and the spin form factor $\Lambda^s_{\mathbf{p},\mathbf{p}'}$ (*30*). The dominant contribution to the $m = \pm 2$ pairing channel comes from the product of the first circular harmonics of D and Λ^s but is somewhat reduced by the product of the second harmonic of D and the zeroth harmonic of Λ^s.

Finally, we discuss the effects of crystal anisotropy. The (110) surface of Bi has a low-symmetry group $\mathbf{D}_1$ with a mirror plane perpendicular to the surface (*18*). Consequently, there are only two symmetry representations, A_1 and A_2, for the superconducting pairing (*23*), which are symmetric and antisymmetric with respect to reflection. The antisymmetric representation A_2 has nodes and is even in $\mathbf{p}$; thus, its wave function is p_xp_y of the d_{xy} type. The symmetric representation A_1 can be of the s or $d_{x^2-y^2}$ type, which belongs to the same representation. Because two different representations, A_1 and A_2, are available, it is possible to make two degenerate time-reversal breaking combinations $d_{xy} \pm id_{x^2-y^2}$ out of them. However, because the A_1 and A_2 representations are not degenerate, their transition temperatures are generally different. Thus, we come to the conclusion that there must be two superconducting transitions in the Bi/Ni bilayers, as in UPt_3 (*4*). We expect that the nodal superconducting state of the d_{xy} type would develop at a higher transition temperature and that the $d_{x^2-y^2}$ state would develop at a lower temperature, spontaneously breaking the TRS by the $d_{xy} \pm id_{x^2-y^2}$ combination and eliminating the nodes. If the crystal anisotropy is weak, the difference between transition temperatures may be small, which may be the reason why the two superconducting transitions have not been resolved so far, but it is an important direction for future experimental studies.

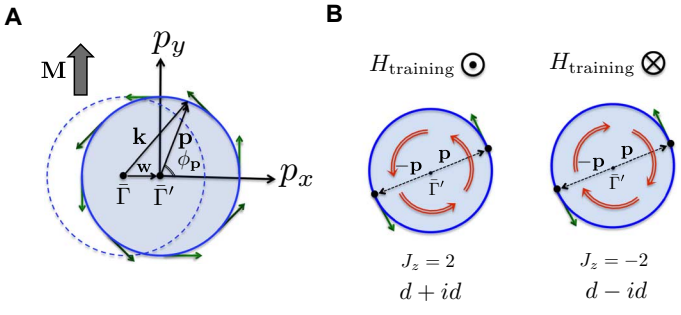

Fig. 3. Shifted Fermi surface and pairing symmetry of Bi electrons. (**A**) The Fermi circle of the electron surface states in Bi. The original dashed blue Fermi circle centered at $\bar{\Gamma}$ is shifted by the vector $\mathbf{w}$ to the solid blue circle (shaded area) centered at $\bar{\Gamma}'$ because of the in-plane magnetization $\mathbf{M}$ produced by Ni. The electron momentum $\mathbf{p}$ is measured from $\bar{\Gamma}'$ and characterized by the azimuthal angle $\phi_\mathbf{p}$. The green arrows show spin polarization locked to the momentum direction. (**B**) Superconducting pairing of the electrons with opposite spins and opposite momenta $\mathbf{p}$ and $-\mathbf{p}$. The TRSB condensate has the total angular momentum $J_z = \pm 2$, corresponding to the $d \pm id$ pairing, as indicated by the red double-curved arrows. A weak training magnetic field can select one of the two degenerate states.

CONCLUSION

In conclusion, we report observation of the PKE in the Bi/Ni epitaxial bilayers, which indicates spontaneous TRSB in the superconducting state.

A combination of strong spin-orbit coupling and noncentrosymmetry makes this 2D interfacial system distinctly different from the bulk TRSB superconductors (*3*–*5*). To describe the TRSB state, we propose a model where magnetic fluctuations in Ni induce superconducting pairing in Bi, with the superconducting phase winding number around the Fermi surface equal to ±2. Thus, Bi/Ni is likely a rare example of a 2D topological superconductor with two chiral edge states moving in the same direction (*23*).

MATERIALS AND METHODS

Setup of the Sagnac interferometer

A schematic of the Sagnac interferometer used in this experiment is shown in fig. S1. In a fiber-optic Sagnac interferometer (*13*), light from a 1550-nm broadband source passed through a polarization-maintaining (PM) circulator and was polarized. A half-wave plate was then used to rotate the polarization axis to 45° with respect to the axis of a phase shift modulator. This modulator added a time-varying phase shift to the light. However, the amplitude of the phase shift and the optical path length were different for the in-plane and out-of-plane polarizations of light. After passing through the modulator, the in-plane and out-of-plane polarizations were no longer coherent with each other, and each polarization beam had a time-varying phase shift of different amplitudes. The light was then routed via a PM fiber to optics mounted on a piezo stage capable of submicrometer step size in both the x and y directions. After exiting the PM fiber, the light was passed through a quarter-wave plate that converted the orthogonal, linear polarizations into left- and right-circular polarizations. Finally, it was focused onto the sample surface. The sample rested inside an optical cryostat with a base temperature of 2.5 K, which contained an optical viewport on the top, allowing the light to pass from the focusing element to the sample surface. Upon reflection from the sample, there was a phase shift between the two polarizations that was twice the size of the Kerr signal. After passing through the quarter-wave plate, the polarization axis of the two beams had been swapped. On the return trip, each beam traveled through the system with a polarization orthogonal to that of its outgoing trip. The net result is that each beam traveled along the exact same optical path but in opposite direction over the round trip. Once each beam passed through the phase shift modulator again, the two beams were once again coherent but had phase differences due to the Kerr effect ($2\theta_K$) as well as the phase shift modulation. The two beams interfered, resulting in an elliptically polarized beam, the in-plane component of which was routed to a photodetector. If ω_m was chosen so that $\tau\omega_m = \pi$, lock-in detection could be used to determine θ_K by comparing the detected signal at ω_m and $2\omega_m$. The dc power received by the photodetector is a measure of the reflectivity of the sample, and the ratio between the signal at $2\omega_m$ and the dc signal is a measure of optical anisotropy, as described in the study by Xia *et al.* (*13*).

Procedure of epitaxially growing samples

All the samples were epitaxially grown in ultrahigh vacuum (UHV), with a base pressure 6×10^{-8} Pa. We first chemically cleaned the MgO(001) substrates before putting them into the UHV chamber. After transfer, we annealed them to 750 K and incubated them at this temperature for 70 min. Figure S2A shows the reflection high-energy electron diffraction (RHEED) patterns for the MgO substrate. The Ni layer was deposited at 300 K, whereas the Bi layer was deposited at 110 K. Figure S2B shows the RHEED patterns of the topmost Bi layer taken at room temperature. The sharp lines indicate that the sample is single crystalline and that the quality is very high, which can also be verified by the cross-sectional scanning transmission electron microscopy image in Fig. 1A.

SUPPLEMENTARY MATERIALS

Supplementary material for this article is available at http://advances.sciencemag.org/cgi/content/full/3/3/e1602579/DC1

Experimental methods and supplementary data

Theory of superconducting pairing in epitaxial bismuth/nickel bilayers

fig. S1. Schematic of Sagnac interferometer.

fig. S2. RHEED patterns of the substrate and the sample.

fig. S3. Supplementary data of the Bi (25 nm)/Ni (2 nm) sample.

fig. S4. Dependence of the critical temperature T_c on the thickness of the Bi and Ni layers.

fig. S5. Kerr signal of the Bi (40 nm)/Ni (2 nm) sample.

fig. S6. Optical signal from the MgO substrate.

References (*31*–*41*)

REFERENCES AND NOTES

1. F. Wilczek, Majorana returns. *Nat. Phys.* **5**, 614 (2009).
2. C. Nayak, S. H. Simon, A. Stern, M. Freedman, S. Das Sarma, Non-Abelian anyons and topological quantum computation. *Rev. Mod. Phys.* **80**, 1083 (2008).
3. J. Xia, Y. Maeno, P. T. Beyersdorf, M. M. Fejer, A. Kapitulnik, High resolution polar Kerr effect measurements of Sr_2RuO_4: Evidence for broken time-reversal symmetry in the superconducting state. *Phys. Rev. Lett.* **97**, 167002 (2006).
4. E. R. Schemm, W. J. Gannon, C. M. Wishne, W. P. Halperin, A. Kapitulnik, Observation of broken time-reversal symmetry in the heavy-fermion superconductor UPt_3. *Science* **345**, 190–193 (2014).
5. E. R. Schemm, R. E. Baumbach, P. H. Tobash, F. Ronning, E. D. Bauer, A. Kapitulnik, Evidence for broken time-reversal symmetry in the superconducting phase of URu_2Si_2. *Phys. Rev. B* **91**, 140506(R) (2015).
6. N. Reyren, S. Thiel, A. D. Caviglia, L. F. Kourkoutis, G. Hammerl, C. Richter, C. W. Schneider, T. Kopp, A.-S. Rüetschi, D. Jaccard, M. Gabay, D. A. Muller, J.-M. Triscone, J. Mannhart, Superconducting interfaces between insulating oxides. *Science* **317**, 1196–1199 (2007).
7. E. Bauer, M. Sigrist, Eds., *Non-centrosymmetric Superconductors,* vol. 847, *Lecture Notes in Physics* (Springer, 2012).
8. N. W. Ashcroft, N. D. Mermin, *Solid State Physics* (Thomson Learning, ed. 2, 1976).
9. J. S. Moodera, R. Meservey, Superconducting phases of Bi and Ga induced by deposition on a Ni sublayer. *Phys. Rev. B* **42**, 179 (1990).
10. P. LeClair, J. S. Moodera, J. Philip, D. Heiman, Coexistence of ferromagnetism and superconductivity in Ni/Bi bilayers. *Phys. Rev. Lett.* **94**, 037006 (2005).
11. X.-X. Gong, H.-X. Zhou, P.-C. Xu, D. Yue, K. Zhu, X.-F. Jin, H. Tian, G.-J. Zhao, T.-Y. Chen, Possible p-wave superconductivity in epitaxial Bi/Ni bilayers. *Chin. Phys. Lett.* **32**, 067402 (2015).
12. A. Kapitulnik, J. Xia, E. Schemm, A. Palevski, Polar Kerr effect as probe for time-reversal symmetry breaking in unconventional superconductors. *New J. Phys.* **11**, 055060 (2009).
13. J. Xia, P. T. Beyersdorf, M. M. Fejer, A. Kapitulnik, Modified Sagnac interferometer for high-sensitivity magneto-optic measurements at cryogenic temperatures. *Appl. Phys. Lett.* **89**, 062508 (2006).
14. S. D. Bader, SMOKE. *J. Magn. Magn. Mater.* **100**, 440–454 (1991).
15. Z. Q. Qiu, S. D. Bader, Surface magneto-optic Kerr effect. *Rev. Sci. Instrum.* **71**, 1243–1255 (2000).
16. E. Taylor, C. Kallin, Intrinsic Hall effect in a multiband chiral superconductor in the absence of an external magnetic field. *Phys. Rev. Lett.* **108**, 157001 (2012).
17. S. Xiao, D. Wei, X. Jin, Bi(111) thin film with insulating interior but metallic surfaces. *Phys. Rev. Lett.* **109**, 166805 (2012).
18. S. Agergaard, C. Søndergaard, H. Li, M. B. Nielsen, S. V. Hoffmann, Z. Li, P. Hofmann, The effect of reduced dimensionality on a semimetal: The electronic structure of the Bi(110) surface. *New J. Phys.* **3**, 15 (2001).
19. Y. M. Koroteev, G. Bihlmayer, J. E. Gayone, E. V. Chulkov, S. Blügel, P. M. Echenique, P. Hofmann, Strong spin-orbit splitting on Bi surfaces. *Phys. Rev. Lett.* **93**, 046403 (2004).
20. J. I. Pascual, G. Bihlmayer, Y. M. Koroteev, H.-P. Rust, G. Ceballos, M. Hansmann, K. Horn, E. V. Chulkov, S. Blügel, P. M. Echenique, P. Hofmann, Role of spin in quasiparticle interference. *Phys. Rev. Lett.* **93**, 196802 (2004).
21. P. Hofmann, The surfaces of bismuth: Structural and electronic properties. *Prog. Surf. Sci.* **81**, 191–245 (2006).
22. Y. M. Koroteev, G. Bihlmayer, E. V. Chulkov, S. Blügel, First-principles investigation of structural and electronic properties of ultrathin Bi films. *Phys. Rev. B* **77**, 045428 (2008).
23. K. V. Samokhin, Symmetry and topology of two-dimensional noncentrosymmetric superconductors. *Phys. Rev. B* **92**, 174517 (2015).

24. L. P. Gor'kov, E. I. Rashba, Superconducting 2D system with lifted spin degeneracy: Mixed singlet-triplet state. *Phys. Rev. Lett.* **87**, 037004 (2001).
25. O. Vafek, L. Wang, Spin-orbit coupling induced enhancement of superconductivity in a two-dimensional repulsive gas of fermions. *Phys. Rev. B* **84**, 172501 (2011).
26. A. Farrell, T. Pereg-Barnea, Zeeman-field-induced nontrivial topology in a spin-orbit-coupled superconductor. *Phys. Rev. B* **90**, 144518 (2014).
27. I. A. Sergienko, S. H. Curnoe, Order parameter in superconductors with nondegenerate bands. *Phys. Rev. B* **70**, 214510 (2004).
28. M. S. Scheurer, Mechanism, time-reversal symmetry, and topology of superconductivity in noncentrosymmetric systems. *Phys. Rev. B* **93**, 174509 (2016).
29. M. Kargarian, D. K. Efimkin, V. Galitski, Amperean pairing at the surface of topological insulators. *Phys. Rev. Lett.* **117**, 076806 (2016).
30. K. V. Samokhin, V. P. Mineev, Gap structure in noncentrosymmetric superconductors. *Phys. Rev. B* **77**, 104520 (2008).
31. T. Hattori, Y. Ihara, Y. Nakai, K. Ishida, Y. Tada, S. Fujimoto, N. Kawakami, E. Osaki, K. Deguchi, N. K. Sato, I. Satoh, Superconductivity induced by longitudinal ferromagnetic fluctuations in UCoGe. *Phys. Rev. Lett.* **108**, 066403 (2012).
32. P. Fulde, R. A. Ferrell, Superconductivity in a strong spin-exchange field. *Phys. Rev.* **135**, A550 (1964).
33. A. I. Larkin, Y. Ovchinnikov, Inhomogeneous state of superconductors. *Sov. Phys. JETP* **20**, 762 (1965).
34. V. Barzykin, L. P. Gor'kov, Inhomogeneous stripe phase revisited for surface superconductivity. *Phys. Rev. Lett.* **89**, 227002 (2002).
35. J. Alicea, Majorana fermions in a tunable semiconductor device. *Phys. Rev. B* **81**, 125318 (2010).
36. F. Loder, A. P. Kampf, T. Kopp, Route to topological superconductivity via magnetic field rotation. *Sci. Rep.* **5**, 15302 (2015).
37. E. Lake, C. Webb, D. A. Pesin, O. A. Starykh, Rashba versus Kohn-Luttinger: Evolution of *p*-wave superconductivity in magnetized two-dimensional Fermi gases subject to spin-orbit interactions. *Phys. Rev. B* **93**, 214516 (2016).
38. A. Steinbok, K. Michaeli, Spontaneous finite momentum pairing in superconductors without inversion symmetry. arXiv: 1602.03194 (2016).
39. Y. Tserkovnyak, D. Loss, Thin-film magnetization dynamics on the surface of a topological insulator. *Phys. Rev. Lett.* **108**, 187201 (2012).
40. P. W. Anderson, Structure of "triplet" superconducting energy gaps. *Phys. Rev. B* **30**, 4000 (1984).
41. J. D. Sau, R. M. Lutchyn, S. Tewari, S. Das Sarma, Generic new platform for topological quantum computation using semiconductor heterostructures. *Phys. Rev. Lett.* **104**, 040502 (2010).

Acknowledgments: V.M.Y. thanks K. Samokhin for the discussion. **Funding:** This study was supported by the NSF (grant DMR-1350122). X.G., D.Y., H.Z., and X.J. acknowledge support from the National Natural Science Foundation of China (grant nos. 11434003 and 11421404) and the National Basic Research Program of China (grant no. 2015CB921402). M.K. and V.M.G. acknowledge support from the U.S. Department of Energy–Basic Energy Sciences (DESC0001911) and the Simons Foundation. **Author contributions:** X.G. took the responsibility of conducting the measurements and analyzing the data. A.S. assisted in the experiment. D.Y. and H.Z. prepared the samples. X.J. developed the Sagnac interferometer. X.J. and J.X. designed the project. M.K. and V.M.Y. conducted the theoretical calculation. J.X., V.M.Y., and V.M.G. wrote the paper. All of the authors contributed to the analysis of the results and the preparation of the manuscript. **Competing interests:** The authors declare that they have no competing interests. **Data and materials availability:** All data needed to evaluate the conclusions in the paper are present in the paper and/or the Supplementary Materials. Additional data related to this paper may be requested from the authors.

Submitted 19 October 2016
Accepted 10 February 2017
Published 31 March 2017
10.1126/sciadv.1602579

Citation: X. Gong, M. Kargarian, A. Stern, D. Yue, H. Zhou, X. Jin, V. M. Galitski, V. M. Yakovenko, J. Xia, Time-reversal symmetry-breaking superconductivity in epitaxial bismuth/nickel bilayers. *Sci. Adv.* **3**, e1602579 (2017).

ScienceAdvances
AAAS

Time-reversal symmetry-breaking superconductivity in epitaxial bismuth/nickel bilayers

Xinxin Gong, Mehdi Kargarian, Alex Stern, Di Yue, Hexin Zhou, Xiaofeng Jin, Victor M. Galitski, Victor M. Yakovenko and Jing Xia

(March 31, 2017)
Sci Adv 2017, 3:.
doi: 10.1126/sciadv.1602579